Structural and functional insights into Cdc45 recruitment by Sld7–Sld3 for CMG complex formation

Hao Li[1], Izumi Ishizaki[1], Koji Kato[1,2,#], XiaoMei Sun[2], Sachiko Muramatsu[3], Hiroshi Itou[3,$], Toyoyuki Ose[1,2], Hiroyuki Araki[3,*], Min Yao[1,2,*]

[1]Graduate School of Life Science, Hokkaido University, Sapporo, 060-0810, Japan.

[2]Faculty of Advanced Life Science, Hokkaido University, Sapporo, 060-0810, Japan.

[3]National Institute of Genetics., Mishima, Shizuoka, 411-8540, Japan

[#]Present address: [Koji Kato] Research Institute for Interdisciplinary Science and Graduate School of Natural Science and Technology, Okayama University, Okayama, 700-8530, Japan

[$]Present address: [Hiroshi Itou] Chiome Bioscience, Inc., Shibuya-ku, Tokyo, 151-0071, Japan

*Correspondence: Min Yao. Tel: +81 (0)11 706 4481 Fax: +81 (0)11 706 4481 Email: yao@castor.sci.hokudai.ac.jp

Correspondence may also be addressed to Hiroyuki Araki. Tel: +81 (0)55 981 6754 Fax: +81 (0)55 981 6762 Email: hiaraki@nig.ac.jp

Keywords: DNA replication, CMG formation, Cdc45 recruitment, Sld3, structure

Abstract

DNA replication requires Cdc45 and GINS recruitment into the MCM duplex hexamer by initiation factors to form an active helicase, the Cdc45–MCM–GINS (CMG) complex, at the replication origins. The initiation factor Sld3 is a central regulator of Cdc45 and GINS recruitment worked with Sld7 together. However, the mechanism through which Sld3 regulates CMG complex formation remains unclear. Here, we present the structure of the Sld3 Cdc45-binding-domain in complex with Cdc45 (Sld3CBD–Cdc45), showing detailed interactions and conformational changes required for binding to each other. The mutant analysis indicated that the binding between Sld3CBD and Cdc45 could be broken easily. We also revealed that Sld3CBD, GINS, and MCM bind to different sites on Cdc45 in the Sld3CDB–CMG model, indicating that after recruitment of Cdc45, Sld7–Sld3 could remain in Cdc45–MCM until CMG formation. The consistency between the particle size of Sld7–Sld3–Cdc45 and the distance between Sld3CBDs in the Cdc45–MCM dimer indicated the binding manner of the Cdc45–Sld3–$[Sld7]_2$–Sld3–Cdc45 off/on MCM duplex hexamer. A DNA-binding assay of Sld3 and its complexes with single-stranded ARS1 fragments revealed a relationship between the dissociation of Sld7–Sld3 from CMG and the unwound single-stranded DNA. These findings help to further our understanding of the molecular basis of regulation of CMG complex formation by Sld3.

Introduction

Eukaryotic chromosomal DNA replication in the cell cycle, a tightly regulated process that ensures precise gene copying, begins with the unwinding of double-stranded DNA (dsDNA) into signal-stranded DNA (ssDNA), including the formation of an active helicase Cdc45–MCM–GINS (CMG) complex [1,2]. In the G1 phase of the yeast cell cycle, two inactive helicase Mcm2–7 hexamer rings (Mcm2–6–4–7–3–5) are loaded onto autonomously replicating sequences (ARSs) of dsDNA to form a double hexamer (MCM DH) at the replication origin [3–5]. To facilitate this loading, Cdt1 binds to the Mcm2–7 hexamer ring and stabilizes a gap formation between the Mcm2 and Mcm5, which serves as a dsDNA entry gate [6–9]. Next, the MCM DH on dsDNA is phosphorylated by Dbf4-dependent protein kinase (Cdc7 kinase or DDK [6F0L]) (Supplementary Figure 1A), allowing the key factor Sld3 and its partner Sld7 to recruit Cdc45 (Sld7–Sld3–Cdc45) to each MCM (Supplementary Figure 1B) [10–13]. Subsequently, the phosphorylation of Sld3 by cyclin-dependent kinase (CDK) regulates the assembly of GINS onto MCM DH with Dpb11, CDK-phosphorylated Sld2, and DNA polymerase ε to form CMG (Supplementary Figure 1C) [14–19]. Finally, the factors Sld2, Sld3, Sld7, and Dpb11 are released by elusive mechanisms from an active CMG and facilitate bidirectional replication by translocating along the 3′ to 5′ direction of the DNA strand (Supplementary Figure 1D) [20, 21].

As a central regulator of CMG formation in *Saccharomyces cerevisiae*, Sld3 functions as a bridge protein in the Sld7–Sld3–Cdc45 complex to recruit Cdc45 to DDK-phosphorylated MCM DH. This Sld3 contains three domains each of which binds mainly to one of Sld7, Cdc45, and MCM. The N-terminal domain of Sld3 (Sld3NTD: M1–L116) binds to the N-terminal domain (M1–D130) of Sld7 (Sld7NTD) (Sld7 C-terminal domain [Sld7CTD: K168–S257] is a self-dimerization domain) [22]. Following the NTD of Sld3, the middle part is a central portion known as the Cdc45-binding domain (Sld3CBD: S148–K430) [12, 23]. A previous study also demonstrated that a region (L510–R530) in the Sld3 C-terminal domain (Sld3CTD: T445–T679) binds to Mcm4 and 6 [24]. CDK-dependent phosphorylation of two residues (T600 and S622) downstream of Sld3CTD initiates the binding of GINS-carrying Dpb11 to Cdc45–MCM [19, 25]. In addition to its role as a bridge in the recruitment of Cdc45 and GINS, Sld3 binds to two ARS1 ssDNA fragments (ssARS1-2 and ssARS1-5) but not to the corresponding dsDNA [26]. The specific association between Sld3 and ssDNA is not affected by CDK phosphorylation. Furthermore, the structures of the Sld7CTD dimer, Sld7NTD–Sld3NTD, Sld3CBD, MCM DH, and CMG were determined through crystallography and cryogenic electron microscopy (cryo-EM). Recent single-molecule biochemical assays have reported the stepwise recruitment of multiple Cdc45s to the MCM DH [27]. However, how Sld3–Sld7 brings Cdc45 into the MCM for the formation of CMG to regulate the initiation of DNA replication remains unclear.

In the present study, we aimed to understand how Sld3 recruits Cdc45 to the MCM DH with Sld7 for CMG formation through structure and particle analyses. The structure of *S. cerevisiae* Sld3CBD–Cdc45 at 2.6 Å resolution presented the detailed interactions between Sld3 and Cdc45, which were confirmed through *in vitro* and *in vivo* mutant analyses. Compared to the monomer structures, the conformation of Sld3CBD and Cdc45 in the Sld3CBD–Cdc45 complex changed significantly to bind each other. Based on the structural similarity of Cdc45s in Sld3CBD–Cdc45 and CMG, we modelled Sld3CBD–Cdc45–MCM–dsDNA and SCMG–dsDNA (Sld3CBD–CMG–dsDNA) as a snapshot of how helicase CMG forms. The models demonstrated that Sld3CBD, MCM, and GINS bind to different sites on Cdc45, indicating that Sld7–Sld3 could remain at Cdc45–MCM until CMG formation after GINS loading. Consistency between the particle size of Sld7–Sld3ΔC–Cdc45, as per spectroscopic analysis, and the distance of Sld3CBDs in the Cdc45–MCM dimer suggested that the ternary complex of Sld7–Sld3–Cdc45 forms a dimer off/on the MCM DH for recruiting Cdc45. Furthermore, ssDNA-binding analysis of ARS1 fragments implied that the release of Sld3–Sld7 could be associated with ssARS1 unwound by CMG. Our findings illustrate the recruit–release function of Sld3 in CMG formation and expand our knowledge of the initiation process of DNA replication.

Results

Overall structure of Sld3CBD and Cdc45 complex

We obtained a recombinant Sld3CBD–Cdc45 complex of *S. cerevisiae* and determined its crystal structure at 2.6 Å resolution using molecular replacement (Supplementary Figure 2 A, Figure 1A). Only one complex exists within an asymmetric unit. Similar to monomer Sld3CBD (PDBID: 3WI3 with RMSD of 0.50 Å for 181 Cα atoms) [23], Sld3CBD (Y154–P420) in the Sld3CBD–Cdc45 complex is an α-helical structure with two disordered regions of R317–S336 and P364–A369, but with a significant difference in that a disordered part in monomer Sld3CBD was visualized as a C-terminal part of bent long helix α8 (F294–R316; referred to as α8CTP) (Supplementary Figures 3A and 4). Cdc45 (M1–L650) is an α/β structure composed of three β-sheets (parallel: β1-β6-β5-β4-β2-β3, anti-parallel: β7-β8, mixed: β10-β11-β12-β14-β13) surrounded by 21 α-helixes. Owing to the poor electron density map, the regions D106–K110, D166–K227, S306–V310, and T438–D460 on the molecular surface could not be built. In contrast to the monomer huCdc45 and the CMG form (Cdc45 in the CMG complex), more than the N-terminal half of the protruding long helix α7 was disordered in the Sld3CBD–Cdc45 complex (Supplementary Figures 3B and 5).

Conformation changes in Sld3CBD and Cdc45 for binding each other

Sld3CBD binds to Cdc45 in a similar way to a toothed gear (Figure 1A right panel), with a contact surface of 1808 $Å^2$ accounting for approximately 13.3% and 7.0% of the total surface of Sld3CBD and Cdc45, respectively. Two helixes (α8 and α9) of Sld3CBD formed a plier structure and gripped the C-terminal domain DHHA1 (R523–L650) of Cdc45 through hydrophobic interactions and hydrogen bonds. The C-terminal loop (L646–L650) and the C-terminal part of α7 (E232–S242) of Cdc45 sandwiched the helix α8CDP of Sld3CBD. Compared to the isolated form (PDBIDs: 5DGO for huCdc45 [28] and 6CC2 for EhCdc45 [29]) and the CMG form (PDBID: 3JC6 [30]), the Cdc45 in the Sld3CBD–Cdc45 complex changed the conformation of DHHA1 to form pockets on its two sides for binding Sld3CBD α8CTP and α9. The remaining part of Cdc45 (~K517) retained a structure with RMSD values of 1.29 Å (isolated huCdc45), 1.81 Å (isolated EhCdc45), and 1.295 Å (in CMG) for 243, 251, and 361 Cα atoms, respectively.

The helix α8CTP (F294–R316) of Sld3CBD was surrounded by the C-terminal domain DHHA1 and a C-terminal part of the protruded long helix α7 (E232–S242) of Cdc45 but completely disordered in Sld3CBD alone (PDBID: 3WI3) [23] (Figure 1A right panel and 1B and Supplementary Figure 3A). Therefore, the helix α8CTP seems to be an intrinsically disordered segment that lacks an ordered conformation alone but folds into a helix coupled to the binding

partner in the Sld3CBD–Cdc45 complex. This α8CTP is essential for binding to Cdc45, as its deletion inhibited cell growth in a previous study [23]. For binding to Sld3CBD α8CTP, loop I595–N604 in Cdc45 DHHA1 changed conformation to interact with Sld3CBD α8CTP. Subsequent the following helix α20 (F605–E615) rotated the C-terminus by 25 degrees, which altered the conformation of the next two β-strands (β13 and β14) in the mixed β-sheet (β10-β11-β12-β14-β13) (Supplementary Figure 3C), allowing Sld3CBD α8CTP to enter the binding pocket. Furthermore, proline substitution for Cdc45 Ser242 (Cdc45-35), which interacts with L307 and T310 in Sld3CBD α8CTP, conferred temperature-sensitive growth to yeast cells (Supplementary Figure 6). Although an increase in the number of copies of Sld3–Sld7 could weakly suppress cell growth defects, it did not recover the disrupted interaction.

The α9 (L337–E360) of Sld3CBD is the secondary Cdc45-binding region (Figure 1C and D and Supplementary Figure 7), which is located in a shallow dent formed by the C-terminal helix and a loop with the following β-strand (K520–Q531) of Cdc45 DHHA1. Three hydrophobic residues (I352, I355, and L356) in Sld3CBD α9 interact with the C-terminal helix (L522, L527, V529, L641, and L647) of Cdc45 DHHA1, while the side chains of two negatively charged residues (D344 and D348) form hydrogen bonds through a water molecule to the main and side chains of R523 on a loop of Cdc45 DHHA1. A disordered region, L527–V529, of Cdc45 DHHA1 in the isolated form forms a β-sheet in the Sld3CBD–Cdc45 complex and binds to the I352 and I355 of Sld3CBD α9. We substituted single, double, or ternary positively charged or hydrophilic residues at D344, D348, I352, I355, and L356 of Sld3CBD α9 (D344R/D348R: Sld3-2R, I352Y: Sld3-Y, I352S/I355S/L356S: Sld3-3S, I352E/I355E/L356E: Sld3-3E). Based on the CD spectra, we confirmed that those mutants keep the structural elements of Sld3CBD (Supplementary Figure 8). Double and ternary mutants Sld3-2R, Sld3-3S, and Sld3-3E eliminated Cdc45-binding affinity, whereas the single mutant Sld3-Y seemed to retain a faint interaction with Cdc45 (Figure 2A). We also substituted the single, double, or ternary residues R523, L522, L527, V529, L637, and L641 of Cdc45 on Sld3CBD α9 binding sites (L637S/L641S: Cdc45-IIS, L637E/L641E: Cdc45-IIE, L522S/L527S/V529S: Cdc45-IIIS, L522E/L527E/V529E: Cdc45-IIIE, and Cdc45-A: R523A). All Cdc45 mutants disrupted the binding between Sld3CDB and Cdc45, except for Cdc45-A, as surmised from the Sld3CBD–Cdc45 structure (Figure 2B). Although mutant Cdc45-A had reduced hydrogen bonds with D344, the remaining hydrogen-bond network maintained contact between Sld3CBD and Cdc45. Furthermore, *in vivo* genetic studies confirmed the importance of these Sld3 residues. By expressing Sld3-3S, Sld3-3E, and Sld3-2R in Sld3, the variant strains caused complete cell death, whereas the Sld3-Y strain maintained cell growth (Figure 2C), indicating that these residues are required to work together to bind Cdc45, and the loss of the Cdc45-binding capacity of Sld3 inhibits the recruitment of Cdc45 and the subsequent formation of the active replicative helicase CMG for DNA replication.

Cdc45 recruitment to MCM DH by Sld3 with partner Sld7

Except for the Sld3 binding region DHHA1, the N-terminal domain of Cdc45 (Cdc45NTD) maintained a structure similar to that of the monomer, Sld3CBD–Cdc45 complex, and CMG complex. Therefore, we modelled Sld3CBD–Cdc45–MCM–dsDNA and SCMG–dsDNA (Figure 3) by superposing Cdc45NTD structures between Sld3CBD–Cdc45 and CMG dimers, which were modelled by superposing Mcm2–7 structures between CMG (PDBID: 3JC6) [30] and MCM–dsDNA (PDBID: 5BK4) [31]. In the models, two Sld3CBDs are located in each monomer of the Cdc45–MCM dimer over 230 Å apart (Figure 3A).

To investigate how Sld7–Sld3 brings Cdc45 to MCM DH, we attempted particle analysis for the Sld7–Sld3-Cdc45 complex using the purified recombinant Sld7–Sld3ΔC–Cdc45. The approximate molecular weight of Sld7–Sld3ΔC–Cdc45 was estimated to be >400 kDa according to size-exclusion chromatography (Supplementary Figure 2B). Given that the molecular weight calculated from their amino acid sequences was 158 kDa, the purified complex should be a dimer. Next, using dynamic light scattering, the particle size (hydrodynamic diameter) of the tripartite complex was estimated to be around 235 Å (Figure 3B, Supplementary Figure 9), which is consistent with the distance of Sld3CBDs in the model of Sld3CBD–Cdc45–MCM dimer. Furthermore, considering that the domains of Sld7 (NTD: Sld3NTD-binding, CTD: self-dimerization) and Sld3 (NTD: Sld7NTD-binding, CBD: Cdc45-binding, CTD: MCM-binding) function independently [22,23], we estimated a dimer model of Sld7–Sld3–Cdc45, as shown in Figure 3B.

Although a previous study showed that Sld3 inhibits the interaction between GINS and MCM by binding experiments [26], our SCMG–dsDNA model demonstrated that Sld3CBD neighbors Mcm2 and binds to Cdc45 on the opposite side of GINS binding (Figure 3C), indicating that Sld7–Sld3 bound to the Cdc45–MCM dimer did not inhibit GINS binding to Cdc45–MCM and could be remained for CMG formation. Interestingly, in the Sld3CBD–Cdc45–MCM–dsDNA and SCMG–dsDNA model, we found that a part (S358-D383) of Sld3CBD containing the C-terminal of α9, a disordered fragment, and α10 was in contact distance with Mcm2CTD. In addition, the Sld3CBD-bound Cdc45 DHHA1 appeared to become close to Mcm2CTD. In contrast, the Cdc45 DHHA1 was not in contact with Mcm2–7 or GINS in the CMG structure (Supplementary Figure 10). The conformational change in Cdc45 DHHA1 not only facilitates binding with Sld3CBD but could also cause contact with Mcm2 without affecting the interaction between Cdc45 and GINS.

ssDNA binding affinity of Sld3 depended on complex formation with Cdc45 and Sld7

Sld3 binds to the ssDNA fragment ARS1, the replication origin [26]. The DNA-binding regions of MCM DH were identified as ssARS1-2 and ssARS1-5 when dsDNA ARS1 was divided into three 80-bp segments (dsARS1-12, dsARS1-34, and dsARS1-56) and unwound to six fragments of ssDNA: ssARS1-1, 2, 3, 4, 5, and 6 (Supplementary Figure 11A). Considering that Sld3 binds to Sld7 and Cdc45 in the MCM–DNA complex, we investigated whether Sld7 and Cdc45 affect the ssDNA-binding capacity of Sld3 to gain more information on the significance of the ssDNA binding of Sld3 during CMG formation. Therefore, we performed an ssDNA binding assay using the Sld3CBD, Sld3CBD–Cdc45, Sld7–Sld3ΔC–Cdc45 and Sld7–Sld3ΔC (Sld3ΔC: binding part M1–N433 to Sld7 and Cdc45) complexes against different regions of ssARS1 for comparison. Cdc45 binds ssDNA with a nonspecific sequence at lengths >60 bases [32]. Therefore, we fragmented each ssARS1 into fragments of 40 bases to prevent this nonspecific interaction (Figure 4A and Supplementary Figures 11B).

For the Sld3CBD and ssDNA mixtures at a molar ratio of 1:1, the band corresponding to ssDNA disappeared, indicating a strong binding affinity (Figure 4B and Supplementary Figures 12). The ssDNA band remained and new bands corresponding to the ssDNA–protein complex appeared when the Sld3CBD–Cdc45 complex was mixed with ssDNA at the same ratio, indicating that the binding affinity of Sld3CBD–Cdc45 for ssDNA was lower than that of Sld3CBD alone (Figure 4B and Supplementary Figures 12). Additionally, the disappearance of ssDNA bands and the appearance of new bands corresponding to the ssDNA–protein complex correlated with an increase in the concentration of Sld3CBD–Cdc45 in the mixture.

In the presence of the Sld7–Sld3ΔC–Cdc45 complex, the band corresponding to ssDNA disappeared in the equimolar ratio of protein and ssDNA, similar to that observed for Sld3CBD (Figure 4B and Supplementary Figures 12). This result demonstrates that the presence of Sld7 could restore the ssDNA-binding capacity of Sld3 to a level comparable to that of Sld3CBD. Also, Sld7–Sld3ΔC showed a ssDNA-binding capacity similar to that of Sld7–Sld3ΔC–Cdc45, implying that ssDNA-binding of Sld7–Sld3ΔC is independent of Cdc45. Furthermore, the results revealed no significant difference in binding affinity between the 40-base fragments of ssARS1-2-1, 2, 3 and ssARS1-5-1, 2, 3 for Sld3CBD, Sld3CBD–Cdc45, and Sld7–Sld3ΔC–Cdc45, indicating that there is no stronger binding-region specific to ssARS1-2 or ssARS1-5 fragments. For sequence specificity, we also analyzed other fragments of ssARS1-1, 3, 4, and 6 and dsARS1, and all of them showed no binding (Supplementary Figure 13). Considering that ssDNA is unwound from dsDNA by the helicase CMG complex, Sld7–Sld3ΔC–Cdc45 and Sld7–Sld3ΔC having a stronger ssDNA-binding capacity than Sld3CBD–Cdc45 imply a relationship between the dissociation of Sld7–Sld3 from the CMG complex and binding to ssDNA unwound by CMG.

Discussion

As a central regulator of helicase CMG formation, Sld3 has attracted interest in studies aiming to understand the initiation of DNA replication. Owing to the lack of structural information on Sld3 complexed with Cdc45 or MCM, how Sld3 regulates helicase activation with other factors remains unknown. Here, we present the structure of the Sld3CBD–Cdc45 complex and particle size of the Sld7–Sld3–Cdc45 complex to examine the detailed mechanisms underlying CMG formation.

Sld3 is highly conserved in eukaryotes, whereas its functional homolog/counterpart in metazoans Treslin (also known as Ticrr) has a distinct size and sequence, except for Sld3CBD. Sequence alignment of Sld3CBD among Sld3 and Treslin revealed that all Cdc45-binding residues in α8 and α9 identified in our study were almost conserved or exhibited conserved changes (Supplementary Figures 4 and 5), indicating that these regions provide a similar mode of interaction between Sld3CBD and Cdc45 in the regulation of metazoan Treslin DNA replication. Therefore, we hypothesize that they load Cdc45, as observed in yeast Sld3 and Sld7.

Sld3CBD and Cdc45 significantly change their conformation to bind to each other in the Sld3CBD–Cdc45 complex compared with their conformation as monomers. Interestingly, the conformational changes in Cdc45 DHHA1 upon binding to Sld3CBD also caused contact with Mcm2NTD in the Sld3CBD–Cdc45–MCM–dsDNA and SCMG–dsDNA models, whereas DHHA1 interacted with neither MCM nor GINS in the CMG structure. Taken together, Sld3CBD contact with Mcm2NTD in the Sld3CBD–Cdc45–MCM–dsDNA and SCMG–dsDNA models and then seems to play a guiding role in helping Cdc45 bind to MCM at the right position. Sld3CBDs in each monomer of the Sld3CBD–Cdc45–MCM dimer were located at a distance of more than 230 Å, which is consistent with the results of a particle size analysis of the Sld7–Sld3ΔC–Cdc45 complex off MCM DH in solution. Therefore, we indicated the binding manner of Sld7–Sld3–Cdc45 in a dimer Cdc45–Sld3–$(Sld7)_2$–Sld3–Cdc45 off/on MCM DH for efficiently recruiting two Cdc45 molecules to an MCM DH, consequently leading to the formation of a pair of CMG helicases.

In the SCMG–dsDNA complex model, Cdc45 bound to Sld3CBD, MCM, and GINS on different sides (with contact surfaces of 6.7, 4.8, and 5.1% of the total Cdc45 surface, respectively), indicating that these bindings occurred independently and did not interfere with each other. In particular, Sld3 and GINS bind to Cdc45 and MCM rings at opposite positions (Mcm2–4–6 and Mcm5–3–7 vs. Sld3 and GINS, respectively), suggesting that the GINS-recruitment protein should cross a long-distance in an MCM monomer or MCM DH to recognize the phosphorylation site (T600 and S622) of Sld3. Furthermore, our SCMG–dsDNA model revealed that Sld3CBD on

CMG appears to contact an N-terminal helix of Mcm2CTD and Sld3CTD could extend to bind to Mcm4NTD through interaction with the NTDs of Mcm2, and 6, rather than the CTD tier (Supplementary Figure 14), indicating that the binding of Sld3–Sld7 to MCM does not appear to affect the ability of AAA+ motors to open and close the MCM ring with a gap between Mcm2CTD and Mcm5CTD [30, 31, 34, 35]. Taking our findings and those of previous studies together, we propose a detailed process for helicase CMG formation from inactive MCM, as depicted in Figure 5 A–C, in which Sld7–Sld3 brings Cdc45 into the MCM as a Sld7–Sld3–Cdc45 dimer (Cdc45–Sld3–$[Sld7]_2$–Sld3–Cdc45), which remains until GINS loading.

The following inquiry concerns the dissociation of Sld3 and other factors. Interestingly, the mutant analysis showed that disrupting just one binding site between Sld3CBD and Cdc45 could cause the dissociation of Sld3CBD and Cdc45, indicating that the binding between Sld3CBD and Cdc45 could be broken easily. Our binding analysis of ssARS1 fragments to Sld3CBD, Sld3CBD–Cdc45, and Sld7–Sld3ΔC–Cdc45 demonstrated the sequence specificity to ssARS1-2 and ssARS1-5 fragments, not others including dsARS1. Considering that ssARS1-2 and ssARS1-5 are on both sides of MCM DH-bound dsDNA [36], and ssARS1-2 disrupts the interaction between Sld3 and Mcm2–7 [26], ssARS1-binding could take advantage of dissociating from CMG for Sld3. As a bridge protein, Sld3 recruits Cdc45 to Sld7, and phosphorylated Sld3 regulates the recruitment of GINS [37]. Finally, the release of Sld3 and Sld7 from CMG could be associated with the binding of ssARS1 unwound by CMG and may also be related to the dissociation of Dpb11–Sld2 from CMG (Figure 5 D, E) [38, 39]. Further structural investigation of Sld3–Sld7–Cdc45–MCM in the GINS-recruiting stage is required to validate the complete CMG formation process.

In conclusion, our structural and biochemical studies of Sld3CBD–Cdc45 revealed a detailed process of CMG formation and the subsequent release of the central regulator Sld3 and other factors associated with single-stranded DNA, leading to a deeper understanding of the initialization mechanism of DNA replication.

Materials and Methods

Preparation of proteins

The C-terminal His-tagged Sld3CBD of *S. cerevisiae* was expressed in *Escherichia coli* and prepared as previously described [23]. For co-expression of *S. cerevisiae* Sld3CBD (S148–K432) and Cdc45 (M1-L650) (Sld3CBD–Cdc45) in *E. coli*, the Sld3CBD DNA fragment containing the His_6-tag (LEHHHHHH) at the C-terminus and the Cdc45 DNA fragment were cloned in the co-overexpression vector pETDuet-1 between the NcoI and SalI restriction sites and the NdeI and XhoI restriction sites, respectively. The primer sequences for Sld3CBD–Cdc45 are listed in Supplementary Table 1.

To confirm the interactions obtained from the Sld3CBD–Cdc45 structure, we constructed four types of single or multi-mutants for Sld3CBD (Sld3-3S: I352S/I355S/L356S, Sld3-3E: 352E/I355E/L356E, Sld3-2R: D344R/D348R, and Sld3-Y: I352Y), and three types of single or multi-mutants for Cdc45 (Cdc45-IIIS: L522S/L527S/V529S, Cdc45-IIIE: L522E/L527E/V529E, Cdc45-IIS: L637S/L641S, Cdc45-IIE: L637E/L641E, and Cdc45-A: R523A) using the Quick Change site-directed mutagenesis method and the inverse PCR method with pETDuet-1–Sld3CBD–Cdc45 as template DNA. The primer sequences for the mutant strains are listed in Supplementary Table 1.

As *S. cerevisiae* Sld7–Sld3–Cdc45 could not be co-overexpressed in *E. coli*, we attempted to clone it from several other fungal sources. The complex of Sld7 (M1-T268), Sld3ΔC (M1-N433), and Cdc45 (M1-I666) from the budding yeast *Kluyveromyces marxianus*, which belongs to the same family as *S. cerevisiae* (Sld7–Sld3ΔC–Cdc45), was cloned into pETDuet-1. We also added a His_6-tag (LEHHHHHH) to the C-terminus of Sld3ΔC. The primer sequences for Sld7–Sld3ΔC and Sld7–Sld3ΔC–Cdc45 are listed in Supplementary Table 1. As Cdc45 mutants can lose the ability to bind to Sld3, we overexpress Sld7–Sld3ΔC by multi-mutants of Cdc45 (Cdc45-IIS) in Sld7–Sld3ΔC–Cdc45. The residues (L654S/L658S) of Cdc45-IIS from *K. marxianus* were selected based on sequence conservation. We constructed mutant Sld7–Sld3ΔC–Cdc45IIS using the Quick Change site-directed mutagenesis method and the inverse PCR method with pETDuet-1–Sld7–Sld3ΔC–Cdc45 as template DNA. The primer sequences for the mutant strains are listed in Supplementary Table 1.

To overexpress Sld3CBD, Sld3CBD–Cdc45, Sld3CBD–Cdc45 mutants, Sld7–Sld3ΔC–Cdc45 and Sld7–Sld3ΔC, the vector of pET26Sld3CBD, pETDuet-1-Sld3CBD–Cdc45, pETDuet-1-Sld3CBD–Cdc45 mutants, pETDuet-1-Sld7–Sld3ΔC–Cdc45 or pETDuet-1-Sld7–Sld3ΔC was transformed into *E. coli* strain BL21 (DE3) through electroporation, followed by preculturing in 5 ml of Luria–Bertani medium containing 100 μg/mL ampicillin at 310 K overnight. The culture was

then transferred to 3 L Luria–Bertani medium and grown until the OD_{600} reached 0.6. After cooling the culture for 30 min on ice, overexpression of each sample was induced by the addition of isopropyl-β-D-1-thiogalactopyranoside to a final concentration of 0.5 mM, and then cells were grown for an additional 12 h at 293 K. Cells were harvested by centrifugation at 4,000 *g* for 20 min at 283 K and then resuspended in a buffer containing 20 mM Tris-HCl pH 7.5, 300 mM NaCl, 10% glycerol, 0.1 mg/ml DNase, and 1× protease-inhibitor cocktail (cOmplete EDTA-free; Roche, Basel, Switzerland).

The harvested cells were crushed through sonication and centrifuged at 40,000 *g* for 30 min at 283 K. After filtration through a 0.45-µm filter (Sigma-Aldrich/Merck Millipore, Burlington, MA, USA), the supernatant was then loaded onto the HisTrap HP column equilibrated with buffer A [20 mM Tris-HCl, pH 7.5, 300 mM NaCl, 10% glycerol], and the column was washed with buffer A. The His-tagged target protein was eluted with imidazole at 20% (100 mM), 30% (150 mM), and 50% (250 mM), followed by a linear gradient of 250–500 mM imidazole in buffer B [20 mM Tris-HCl, pH 7.5, 300 mM NaCl, 10% glycerol, 500 mM imidazole]. We analyzed the fractions using sodium dodecyl sulfate-polyacrylamide gel electrophoresis (SDS-PAGE). Except for mutants of Sld3CBD–Cdc45, the pooled fractions were then purified through size-exclusion chromatography using a buffer A-equilibrated Superdex 200 16/60 column (GE HealthCare, Chicago, IL, USA). Protein purity was confirmed through SDS-PAGE. The purified samples were concentrated to 10 mg/ml and stored at 193 K.

Crystallization and diffraction data collection

The crystallization screening of Sld3CBD–Cdc45 was performed at 293 K using the sitting-drop vapor diffusion method. The drop was a mixture of 1.0 µl of a 10 mg/ml protein solution with the equivalent volume of reservoir buffer from the commercial crystallization kits (JCSG core I-IV, classics, classics II, PEGs, PEGsII, and MPD suite from Qiagen, Venlo, the Netherlands). The initial needle- and plate-shaped crystals appeared under eight and one conditions, respectively. After optimizing the conditions by altering the type and concentration of precipitant, the salt reagent, and the pH of the buffer, the best crystals were obtained in a solution of 0.2M sodium acetate, 0.1M Bis-Tris propane (pH 6.5: pH 8.5 = 3:7), 20%(w/v) PEG3500, and a drop containing 2.0 µl of a 10 mg/ml protein solution mixed with the equivalent volume of reservoir buffer.

Diffraction data were collected using a beamline BL-17A at the Photon Factory, Tsukuba, Japan. Before data collection, the crystals were cryoprotected by soaking them in a reservoir buffer supplemented with 5% (v/v) glycerol and then flash-cooled under a nitrogen gas stream at 100 K. *XDS/XSCALE* was used to index, integrate, scale, and merge the dataset [40]. Supplementary Table 2 summarizes the data collection and data processing statistics.

Structure determination and refinement

The structure of Sld3CBD–Cdc45 was determined using the molecular replacement method with the *AutoMR* wizard in *Phenix* [41, 42] and human Cdc45 (PDBID: 5DGO) [28] and Sld3CBD (PDBID:3WI3) [1] structures were used as search models. Several rounds of refinement were performed using the *Phenix_refine* program in *Phenix*, interleaved with manual building and fitting according to the electron density maps of 2Fo-Fc and Fo-Fc using the *Coot* program [43, 44]. Supplementary Table 2 shows the final refinement statistics and geometry defined by MolProbity [45]. All structural diagrams were generated using *PyMol* [46].

Mutant analysis of Sld3 and Cdc45

We constructed four variants of Sld3CBD and three variants of Cdc45 according to the binding information from the obtained Sld3CBD–Cdc45 structure. After extracting the samples through Ni-affinity chromatography using a HisTrap HP column, we checked the binding status of the mutants using SDS-PAGE.

To check whether mutations affected the structure, we performed circular dichroism (CD) spectrometry measurement of Sld3mutants–Cdc45. CD spectra were collected using a J-805 spectropolarimeter (JASCO, Tokyo, Japan) in a quartz cell with a path length of 1 mm in an atmosphere of N_2 at 298K. For CD measurements, the samples were dialyzed in a buffer [20 mM Tris-HCl, pH 7.5, 50 mM NaCl] and adjusted to a concentration of 0.5 mg/mL through absorption. CD spectra for the wavelength range of 190–300 nm were obtained by averaging the results of four scans. The results are given in molar ellipticity per residues [θ] mrw ($\times 10^{-3}$) vs the wavelength/nm [47]. The secondary structures of each sample were estimated using the K2D3 method [48]. For wild-type Sld3CBD, we calculated secondary structures from the obtained Sld3CBD–Cdc45 structure.

Growth of mutant cells

The isolation and plasmid shuffling of the temperature-sensitive yeast strain YYK13 (for Sld3 mutant analysis) and Cdc45-35 (for Cdc45 mutant analysis) have been described in a previous study [12]. To investigate Sld3 mutants, strain YYK13 was transformed with the YCplac22 plasmid containing multiple variants of *SLD3* mutant genes. The transformants were streaked on SD plates lacking Trp and Leu (SD-Trp, Leu) and SD-Trp, Leu containing 5-fluoroorotic acid (5-FOA-Trp, Leu), and then incubated at 298 K for 3 days. To analyze the Cdc45 mutant, strain Cdc45-35 containing the *CDC45* mutant gene was re-transformed with the YEplac195 plasmid containing *SLD3* and the YEplac122 plasmid containing *SLD7*. The transformants were streaked on yeast extract–peptone–dextrose plates and incubated at 298 or 305 K for 3 days.

Modelling of complexes

We constructed the models of Sld3CBD–Cdc45–MCM–dsDNA (Sld3CBD–Cdc45–MCM dimer complexed with dsDNA) and SCMG–dsDNA (SCMG dimer complexed with dsDNA) using a two-step process. First, the structure of the MCM–NTDs in the CMG monomer (PDBID: 3JC6) [30] was superimposed on that of MCM DH complexed with dsDNA (5BK4) [31] to obtain a dimer of Cdc45–MCM–GINS complexed with dsDNA (Cdc45–MCM–GINS–dsDNA). Next, the models of Sld3CBD–Cdc45–MCM–dsDNA and SCMG–dsDNA were obtained by superimposing Cdc45NTD from Sld3CBD–Cdc45 onto Cdc45–MCM–GINS–dsDNA.

Dynamic light scattering

We estimated the particle size of the Sld7–Sld3ΔC–Cdc45 complex using dynamic light scattering in the term of peak size [49]. To avoid the effect of concentration, we measured four samples of the Sld7–Sld3ΔC–Cdc45 complex. Each sample was overexpressed independently and purified through size-exclusion chromatography. All samples were concentrated to 10 mg/ml, and stored at 193 K. Before measurement, protein samples were dialyzed in a buffer containing 20 mM Tris-HCl pH 7.5 and 300 mM NaCl and then filtered through a 0.22-μm filter. Dynamic light scattering data were collected and analyzed using a Malvern Zetasizer Nano-ZS instrument (Malvern Panalytical, Malvern, UK) for 0.2–0.5 mg/ml protein samples 500 μl in a microquartz cuvette (Malvern-ZEN0112). An automatic duration model was used to collect data. The Zetasizer 6.20 was utilized for data analysis form three measurements to estimate the particle size of each sample.

Electrophoretic mobility shift assay for ssDNA binding

Sld3 binds to single strands of DNA (*ssARS1-2* and *ssARS1-5*) [26]. To determine the specificity of the ssDNA binding affinity of Sld3, we conducted an electrophoretic mobility shift assay (EMSA) using non-denaturing PAGE (native-PAGE) [50]. Given that Cdc45 binds ssDNA with a nonspecific sequence at lengths greater than 60 bases [32], we designed three fragments of ssDNA 40 bases in length (first half 1–40 bp, second half 41–80 bp, and middle half 21–60 bp) for each ssDNA 80-bp segment. All ssDNA fragments of *S. cerevisiae* were synthesized by Sigma-Aldrich. The 40-bp dsDNA fragments (dsARS1-34_1:ssARS1-3_1/ssARS1-4_2) were converted by annealing them using the PCR protocol and then checked through SDS-PAGE. The loaded samples were incubated overnight at 277 K in TMK buffer containing synthesized ssDNA and varying amounts of proteins at ssDNA: protein molecular ratios of 1:0, 1:1, 1:2, 1:4, and 0:1. After incubation, the mixtures were loaded onto a polyacrylamide gel (5% (w/v) acrylamide (39:1), 10% 10 × running buffer (0.25 M Tris, 1.92 M Glycine), 0.1% Ammonium peroxodisulphate,

0.06% (v/v) TEMED) without denaturing (native-PAGE). EMSA was performed at 10 mA/200 V per gel for 40 min at 277 K in 1 × running buffer. After electrophoresis, the reaction products were visualized using SYBR safe (SYBR safe:1 × running buffer = 0.0001:1) to stain the ssDNA and Coomassie brilliant blue (G-250) to stain the proteins. We repeated the EMSA experiments three or more times to confirm the readability. Considering the functional similarity of ARS1-core, the EMSA of Sld7–Sld3ΔC and Sld7–Sld3ΔC–Cdc45 of *K. marxianus* used ssDNA fragments of *S. cerevisiae*.

Data Availability:

Structures and associated experimental data for Sld3CBD-Cdc45 complex (8J09) were deposited in the Protein Data Bank Japan.

Author Contributions: Hao Li: Investigation, Formal analysis, Writing—original draft & editing. Izumi Ishizaki: Investigation, Formal analysis. Koji Kato: Formal structure analysis. XiaoMei Sun: Investigation. Sachiko Muramatsu: Investigation. Hiroshi Itou: Investigation, Writing—review & editing. Toyoyuki Ose: Formal analysis. Hiroyuki Araki: conceptualization, Formal analysis, Writing—review & editing. Min Yao: conceptualization, Formal analysis, Methodology, Writing—original draft & editing.

Acknowledgments

The authors thank Mr. Naofumi Sakurai for his help in the purification of proteins. We would like to thank the beamline staff of the Photon Factory and SPring-8 for collecting X-ray diffraction data (Proposal No. 2016A2562, 2017A2551, and 2018A2508)

Funding

This work was supported by KAKENHI Grant-in-aid for Scientific Research(B), Japan Society for the Promotion of Science [No. 21H01754 to M. Y.]; and Platform Project for Supporting Drug Discovery and Life Science Research, Japan Agency for Medical Research and Development [JP18am0101071, JP19am0101083].

References

1. Tanaka S., Araki H. Helicase activation and establishment of replication forks at chromosomal origins of replication. *Cold Spring Harbor perspectives in biology*. 5: a010371 (2013).
2. Costa A., Diffley J. F. The initiation of eukaryotic DNA replication. *Annual Review of Biochemistry*. 91:107-131 (2022).
3. Evrin C., Clarke P., Zech J., Lurz R., Sun J., Uhle S., Li H., Stillman B., Speck C. A double-hexameric MCM2-7 complex is loaded onto origin DNA during licensing of eukaryotic DNA replication. *Proceedings of the National Academy of Sciences*. 106:20240-20245 (2009).
4. Remus D., Beuron F., Tolun G., Griffith J. D., Morris E. P., Diffley J. F. Concerted loading of Mcm2–7 double hexamers around DNA during DNA replication origin licensing. *Cell*. 139:719-730 (2009).
5. Ticau S., Friedman L. J., Champasa K., Corrêa Jr I. R., Gelles J., Bell S. P. Mechanism and timing of Mcm2–7 ring closure during DNA replication origin licensing. *Nature structural & molecular biology*. 24:309-315 (2017).
6. Samel S. A., Fernández-Cid A., Sun J., Riera A., Tognetti S., Herrera M. C., Li H., Speck, C. A unique DNA entry gate serves for regulated loading of the eukaryotic replicative helicase MCM2–7 onto DNA. *Genes & development*. 28:1653-1666 (2014).
7. Zhai Y., Cheng E., Wu H., Li N., Yung P. Y. K., Gao, N., Tye, B. K. Open-ringed structure of the Cdt1–Mcm2–7 complex as a precursor of the MCM double hexamer. *Nature structural & molecular biology*. 24:300-308 (2017).
8. Bochman M. L., Bell S. P., Schwacha A. Subunit organization of Mcm2-7 and the unequal role of active sites in ATP hydrolysis and viability. *Molecular and cellular biology*. (2008).
9. Frigola J., He J., Kinkelin K., Pye V. E., Renault L., Douglas M. E., Remus D., Cherepanov P., Costa A., Diffley, J. F. X. Cdt1 stabilizes an open MCM ring for helicase loading. *Nature communications*. 8:15720 (2017).
10. Tanaka T., Umemori T., Endo S., Muramatsu S., Kanemaki M., Kamimura Y., Obuse C., Araki, H. Sld7, an Sld3-associated protein required for efficient chromosomal DNA replication in budding yeast. *The EMBO journal*. 30:2019-2030 (2011).
11. Heller R. C., Kang S., Lam W. M., Chen S., Chan C. S., Bell S. P. Eukaryotic origin-dependent DNA replication in vitro reveals sequential action of DDK and S-CDK kinases. *Cell*. 146:80-91 (2011).
12. Kamimura Y., Tak Y. S., Sugino A., Araki, H. Sld3, which interacts with Cdc45 (Sld4), functions for chromosomal DNA replication in Saccharomyces cerevisiae. *The EMBO journal*. 20:2097-2107 (2001).

13. Nakajima R., Masukata H. SpSld3 is required for loading and maintenance of SpCdc45 on chromatin in DNA replication in fission yeast. *Molecular biology of the cell*. 13:1462-1472 (2002).
14. Dhingra N., Bruck I., Smith S., Ning B., Kaplan D. L. Dpb11 protein helps control assembly of the Cdc45· Mcm2-7· GINS replication fork helicase. *Journal of Biological Chemistry*. 290:7586-7601 (2015).
15. Choi J. M., Lim H. S., Kim J. J., Song O. K., Cho, Y. Crystal structure of the human GINS complex. *Genes & Development*. 21:1316-1321 (2007).
16. Bruck I., Kanter D. M., Kaplan, D. L. Enabling association of the GINS protein tetramer with the mini chromosome maintenance (Mcm) 2–7 protein complex by phosphorylated Sld2 protein and single-stranded origin DNA. *Journal of Biological Chemistry*. 286:36414-36426 (2011).
17. Masumoto H., Muramatsu S., Kamimura Y., Araki, H. S-Cdk-dependent phosphorylation of Sld2 essential for chromosomal DNA replication in budding yeast. *Nature*. 415:651-655 (2002).
18. Tanaka S., Komeda Y., Umemori T., Kubota Y., Takisawa H., Araki H. Efficient initiation of DNA replication in eukaryotes requires Dpb11/TopBP1-GINS interaction. *Molecular and cellular biology*. 33: 2614-2622 (2013).
19. Tanaka S., Umemori T., Hirai K., Muramatsu S., Kamimura Y., Araki, H. CDK-dependent phosphorylation of Sld2 and Sld3 initiates DNA replication in budding yeast. *Nature*. 445:328-332 (2007).
20. Costa A., Ilves I., Tamberg N., Petojevic T., Nogales E., Botchan M. R., Berger, J. M. The structural basis for MCM2–7 helicase activation by GINS and Cdc45. *Nature structural & molecular biology*. 18:471-477 (2011).
21. Szambowska A., Tessmer I., Kursula P., Usskilat C., Prus P., Pospiech H., Grosse F. DNA binding properties of human Cdc45 suggest a function as molecular wedge for DNA unwinding. *Nucleic acids research*. 42:2308-2319 (2014).
22. Itou H., Shirakihara Y., Araki, H. The quaternary structure of the eukaryotic DNA replication proteins Sld7 and Sld3. *Acta Crystallographica Section D: Biological Crystallography*. 71:1649-1656 (2015).
23. Itou H., Muramatsu S., Shirakihara Y., Araki, H. Crystal structure of the homology domain of the eukaryotic DNA replication proteins Sld3/Treslin. *Structure*. 22:1341-1347 (2014).
24. Deegan T. D., Yeeles J. T., Diffley, J. F. Phosphopeptide binding by Sld3 links Dbf4-dependent kinase to MCM replicative helicase activation. *The EMBO journal*. 35:961-973 (2016).

25. Zegerman P., & Diffley J. F. Phosphorylation of Sld2 and Sld3 by cyclin-dependent kinases promotes DNA replication in budding yeast. *Nature*. 445:281-285 (2007).
26. Bruck I., Kaplan D. L. Origin single-stranded DNA releases Sld3 protein from the Mcm2–7 complex, allowing the GINS tetramer to bind the Mcm2–7 complex. *Journal of Biological Chemistry*. 286:18602-18613 (2011).
27. De Jesús-Kim L., Friedman L. J., Lõoke M., Ramsoomair C. K., Gelles J., Bell, S. P. DDK regulates replication initiation by controlling the multiplicity of Cdc45-GINS binding to Mcm2-7. *Elife*. 10:e65471 (2021).
28. Simon A. C., Sannino V., Costanzo V., Pellegrini L. Structure of human Cdc45 and implications for CMG helicase function. *Nature communications*. 7:11638 (2016).
29. Kurniawan F., Shi K., Kurahashi K., Bielinsky A. K., Aihara H. Crystal structure of Entamoeba histolytica Cdc45 suggests a conformational switch that may regulate DNA replication. *Iscience*. 3:102-109 (2018).
30. Yuan Z., Bai L., Sun J., Georgescu R., Liu J., O'donnell M. E., Li H. Structure of the eukaryotic replicative CMG helicase suggests a pumpjack motion for translocation. *Nature structural & molecular biology*. 23:217-224 (2016).
31. Noguchi Y., Yuan Z., Bai L., Schneider S., Zhao G., Stillman B., Speck C., Li H. Cryo-EM structure of Mcm2-7 double hexamer on DNA suggests a lagging-strand DNA extrusion model. *Proceedings of the National Academy of Sciences*. 114:E9529-E9538 (2017).
32. Bruck I., Kaplan D. L. Cdc45 protein-single-stranded DNA interaction is important for stalling the helicase during replication stress. *Journal of Biological Chemistry*. 288:7550-7563 (2013).
33. Newlon C. S., Theis J. F. The structure and function of yeast ARS elements. *Current opinion in genetics & development*. 3:752-758 (1993).
34. Li N., Zhai Y., Zhang Y., Li W., Yang M., Lei J., Tye B., Gao N. Structure of the eukaryotic MCM complex at 3.8 Å. *Nature*. 524:186-191 (2015).
35. Abid Ali F., Renault L., Gannon J., Gahlon H. L., Kotecha A., Zhou J. C., Rueda D., Costa A. Cryo-EM structures of the eukaryotic replicative helicase bound to a translocation substrate. *Nature communications*. 7:10708 (2016).
36. Chang F., May C. D., Hoggard T., Miller J., Fox C. A., Weinreich M. High-resolution analysis of four efficient yeast replication origins reveals new insights into the ORC and putative MCM binding elements. *Nucleic acids research*. 39:6523-6535 (2011).
37. Muramatsu S., Hirai K., Tak Y. S., Kamimura Y., Araki H. CDK-dependent complex formation between replication proteins Dpb11, Sld2, Pol □, and GINS in budding yeast. *Genes & development*. 24:602-612 (2010).

38. Lewis J. S., Gross M. H., Sousa J., Henrikus S. S., Greiwe J. F., Nans A., Diffley J.F.X., Costa A. Mechanism of replication origin melting nucleated by CMG helicase assembly. *Nature*. 606:1007-1014 (2022).
39. Douglas M. E., Ali F. A., Costa A., Diffley J. F. The mechanism of eukaryotic CMG helicase activation. *Nature*. 555:265-268 (2018).
40. Kabsch W. Integration, scaling, space-group assignment and post-refinement. *Acta Crystallographica Section D: Biological Crystallography*. 66:133-144 (2010).
41. McCoy A. J., Grosse-Kunstleve R. W., Adams P. D., Winn M. D., Storoni L. C., Read R. J. Phaser crystallographic software. *Journal of applied crystallography*. 40:658-674 (2007).
42. Adams P. D., Afonine P. V., Bunkóczi G., Chen V. B., Davis I. W., Echols N., Headd J. J., Hung L., Kapral G. J., Grosse-Kunstleve R.W., et al. PHENIX: a comprehensive Python-based system for macromolecular structure solution. *Acta Crystallographica Section D: Biological Crystallography*. 66: 213-221 (2010).
43. Emsley P., Cowtan K. Coot: model-building tools for molecular graphics. *Acta crystallographica section D: biological crystallography*. 60:2126-2132 (2004).
44. Chen V. B., Arendall W. B., Headd J. J., Keedy D. A., Immormino R. M., Kapral G. J., Murray L. W., Richardson J. S., Richardson D. C. MolProbity: all-atom structure validation for macromolecular crystallography. *Acta Crystallogr D.* 66:12-21 (2010).
45. DeLano W. L. Pymol: An open-source molecular graphics tool. *CCP4 Newsl. Protein Crystallogr*. 40:82-92 (2002).
46. Abid Ali F., Douglas M. E., Locke J., Pye V. E., Nans A., Diffley J. F., Costa A. Cryo-EM structure of a licensed DNA replication origin. *Nature communications*. 8:2241 (2017).
47. Greenfield N. J. Using circular dichroism spectra to estimate protein secondary structure. *Nature protocols.* 1:2876-2890 (2006).
48. Louis-Jeune C., Andrade-Navarro M. A., Perez-Iratxeta C. Prediction of protein secondary structure from circular dichroism using theoretically derived spectra. *Proteins: Structure, Function, and Bioinformatics*. 80:374-381 (2012).
49. Stetefeld J., McKenna S. A., Patel T. R. Dynamic light scattering: a practical guide and applications in biomedical sciences. *Biophysical reviews.* 8: 409-427 (2016).
50. Hellman L. M., Fried M. G. Electrophoretic mobility shift assay (EMSA) for detecting protein–nucleic acid interactions. *Nature protocols*. 2:1849-1861 (2007).

Figures and Tables

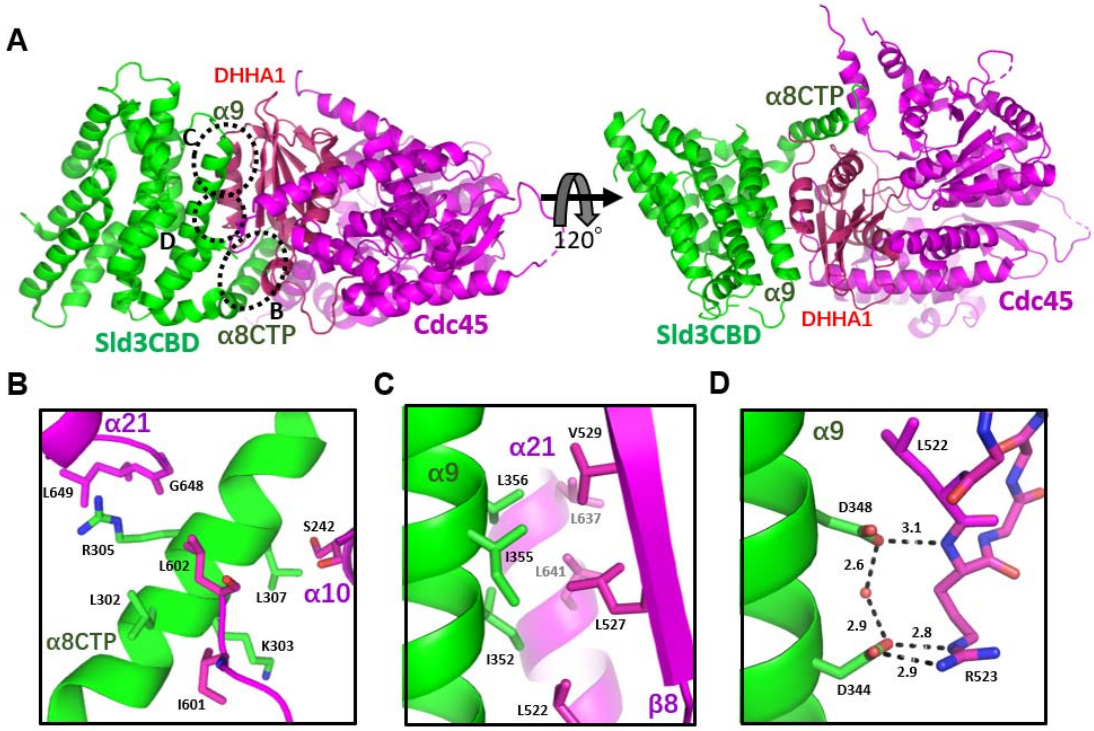

Figure 1. Sld3CBD–Cdc45 complex structure

(A) Structure of the Sld3CBD–Cdc45 complex. Dotted circles B, C, and D mark three binding sites, corresponding to the bottom panel. Proteins Sld3CBD and Cdc45 are colored in green and magenta, respectively. The DHHA1 of Cdc45 is labeled and colored in dark magenta. (B) Binding site on the α8CTP of Sld3CBD. In (C) and (D), two binding sites involving hydrophobic and hydrogen-bond interactions on the α9 of Sld3CBD, respectively. The interacted residues are depicted by sticks and labelled. The black dotted lines show hydrogen bonds.

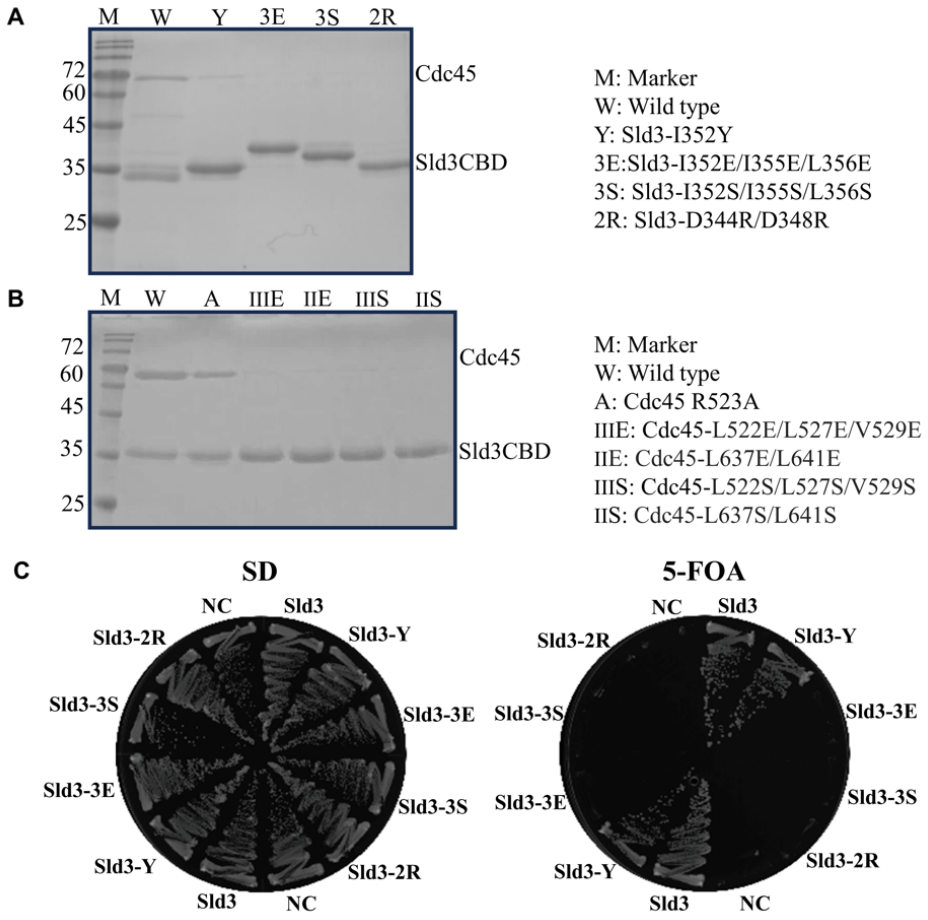

Figure 2. Mutation analysis of interacted residues

(A) *In vitro* binding analysis was checked using SDS-PAGE after Ni-affinity chromatography extraction of co-overexpressed Cdc45 with each Sld3 mutant. Sld3 was tagged by His-tag to bind to the column. The labels M, W, Y, 3E, 3S, and 2R are explained on the right. (B) *In vitro* binding analysis was checked using SDS-PAGE after Ni-affinity chromatography extraction of co-overexpressed Sld3 with each Cdc45 mutant. Sld3 was tagged by His-tag to bind to the column. The labels M, W, A, IIIE, IIE, IIIS, and IIS are explained on the right. (C) *In vivo* cell growth analysis of yeast cells carrying *sld3* mutations. The yeast YYK13 cells carrying *SLD3* or its mutant plasmids were streaked onto SD and FOA plates and then incubated at 298 K for 3 days. YYK13 yeast is a mutant lacking the *SLD3* gene with added *SLD3*/*sld3* mutant gene (YCplac22 plasmid containing *SLD3* or *sld3* mutant) that grew on SD and FOA plates. The empty plasmids were used as negative control (NC). Mutations in Sld3-Y, Sld3-3E, Sld3-3S, and Sld3-2R are the same as those in A.

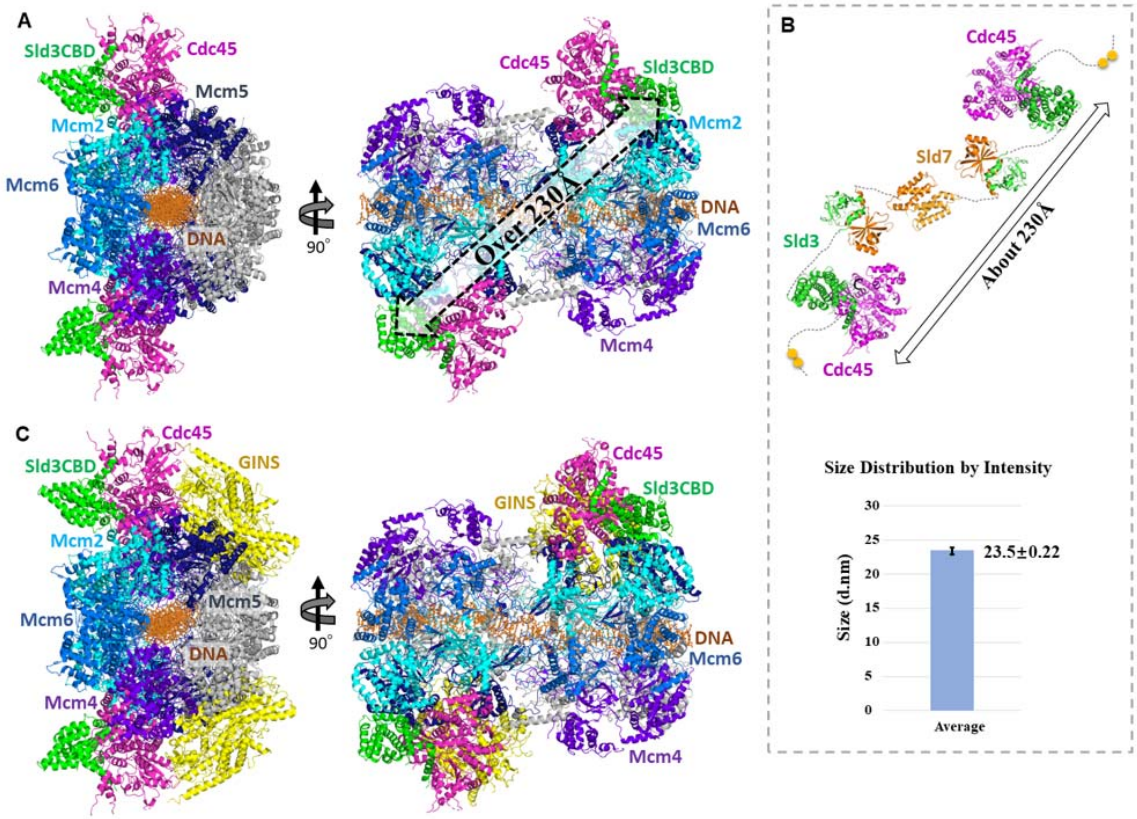

Figure 3. Ribbon models of complexes in dimer form and particle analysis

(A) Sld3CBD–Cdc45–MCM–dsDNA complex. Mcm2, 5, 4, and 6 subunits are colored in cyan, blue, marine, and light blue, respectively. Subunits Mcm3 and Mcm7 are colored in gray. Green and pink are used to color Sld3CBD and Cdc45, respectively. dsDNA is represented by a dark-orange stick. (B) Sld3CBD–Sld7–Cdc45 dimer before associating with the MCM DH. Sld3 and Cdc45 are shown in the same color as they are in A, while Sld7 is colored in orange. The two phosphorylated Sld3 residues are depicted as yellow balls. Particle analysis of Sld7–Sld3ΔC–Cdc45 through dynamic light scattering is shown on the bottom panel. The average peak size of the particle size distribution of the Sld7–Sld3ΔC–Cdc45 complex was estimated to be 23.5 Å in diameter. The measurement was carried out independently four times (Supplementary Figure 9). (C) SCMG–dsDNA complex. GINS is shown in yellow and the remainder are colored identically to those in A and B.

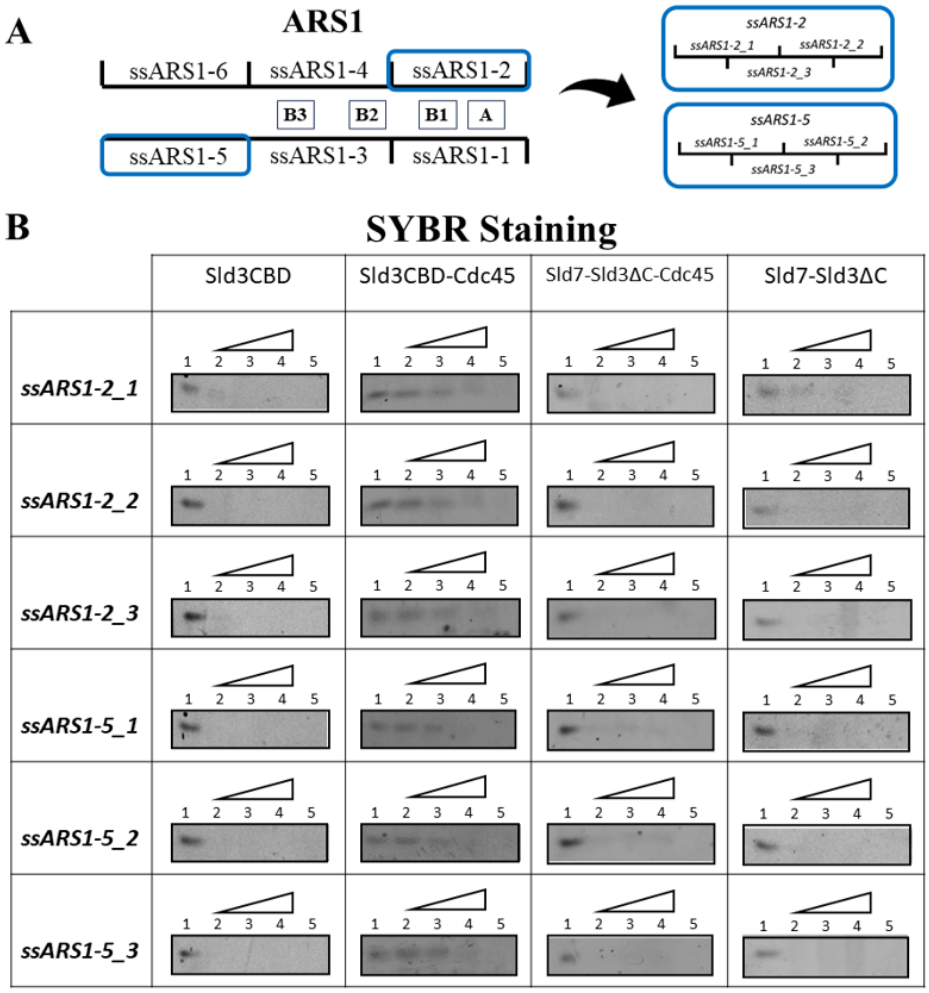

Figure 4. Electrophoresis mobility shift assay (EMSA) of ssDNA binding to Sld3 and its complexes with Sld7 and Cdc45

(A) Schematic of ssARS1-1–ssARS1-6. The important elements of A (ARS consensus sequence), B1, B2, and B3 for unwinding are marked [33]. We divided ssARS1-2 and ssARS1-5 fragments (blue squares) into 40-base lengths for EMSA. (B) ssDNAs were visualized using SYBR safe on polyacrylamide gels. In the presence of ssDNA fragments, Sld3CBD, Sld3CBD–Cdc45, Sld7–Sld3ΔC–Cdc45 and Sld7–Sld3ΔC were incubated with molecular mass-related concentrations. The molecular ratio of ssDNA to protein in lanes 1, 2, 3, 4, and 5 was 1:0, 1:1, 1:2, 1:4, and 0:1, respectively. The controls for ssDNA and protein are lanes 1 and 5, respectively. The disappearance of the ssDNA band in lanes 2–5 indicates that the protein (Sld3CBD, Sld7–Sld3ΔC and Sld7–Sld3ΔC–Cdc45) binds with high affinity.

Figure 5

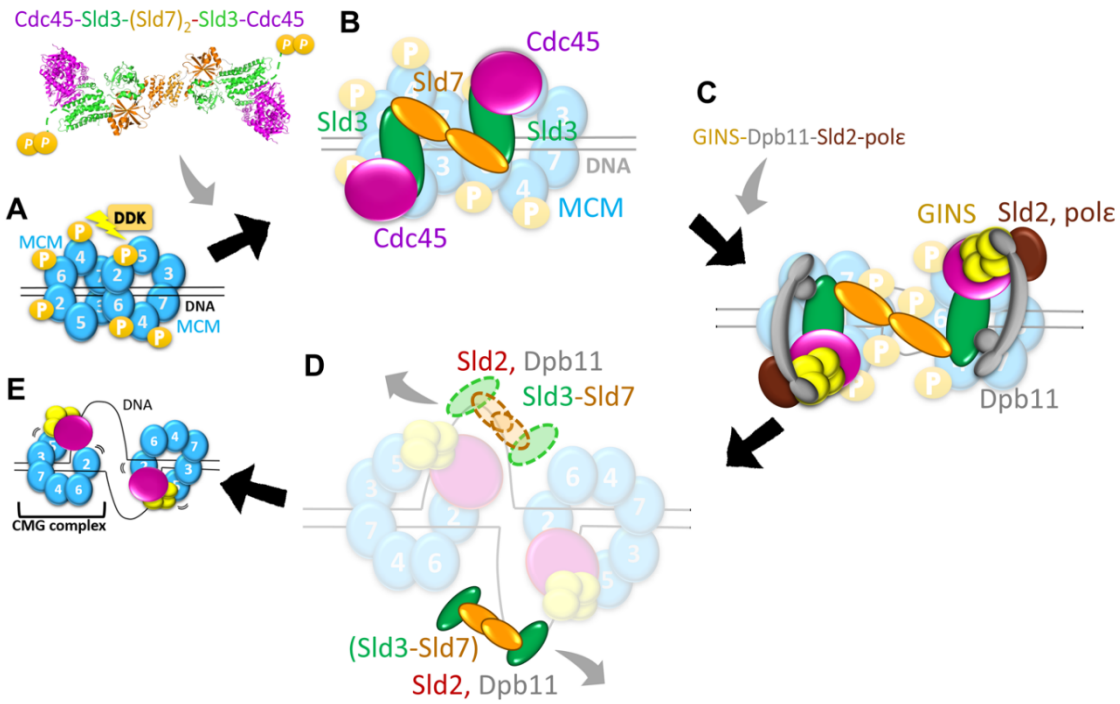

Figure 5. Proposal for CMG formation with Sld7–Sld3

(A) Phosphorylation of Mcm2,4,6 by DDK after MCM DH was loaded on dsDNA at the replication origin. (B) Cdcd45 recruitment to MCM DH by Cdc45–Sld3–$[Sld7]_2$–Sld3–Cdcd45. (C) After CDK-mediated phosphorylation of Sld3CTD in Cdc45–MCM, Dpb11–Sld2 recruits GINS and polε to Sld7–Sld3-Cdc45–MCM to form an active helicase CMG. (D) Unwinding of dsDNA by CMG with MCM DH separation and MCM ring opening. Sld3 and other factors are released upon binding to ssDNA. (E) Each CMG unwinds the dsDNA in two directions, initiating DNA replication.